# Kinetic modelling and molecular dynamics simulation of ultracold neutral plasmas including ionic correlations

T. Pohl, T. Pattard, and J.M. Rost

Max Planck Institute for the Physics of Complex Systems,

Nöthnitzer Str. 38, D-01187 Dresden, Germany

(Dated: November 6, 2018)

# Abstract

A kinetic approach for the evolution of ultracold neutral plasmas including interionic correlations and the treatment of ionization/excitation and recombination/deexcitation by rate equations is described in detail. To assess the reliability of the approximations inherent in the kinetic model, we have developed a hybrid molecular dynamics method. Comparison of the results reveals that the kinetic model describes the atomic and ionic observables of the ultracold plasma surprisingly well, confirming our earlier findings concerning the role of ion-ion correlations [Phys. Rev. A 68, 010703]. In addition, the molecular dynamics approach allows one to study the relaxation of the ionic plasma component towards thermodynamical equilibrium.

PACS numbers: 52.20.-j, 32.80.Pj, 52.25.Dg, 52.65.Ww

#### I. INTRODUCTION

Recent experiments have produced ultracold neutral plasmas from a small cloud of laser-cooled atoms confined in a magneto-optical trap [1, 2, 3, 4, 5, 6]. In one type of experiments [1, 2, 3], a plasma was produced by photoionizing laser-cooled Xe atoms with an initial ion temperature of about  $10\,\mu\text{K}$ . By tuning the frequency of the ionizing laser, the initial electron energy  $E_{\rm e}$  could be varied corresponding to a temperature range  $1\,\text{K} < E_{\rm e}/k_{\rm B} < 1000\,\text{K}$ , and the subsequent expansion of the plasma into the surrounding vacuum was studied systematically. In a complementary type of experiment [4, 5, 6], ultracold Rb and Cs atoms were laser-excited into high Rydberg states rather than directly ionized. In these experiments, also the spontaneous evolution of the Rydberg gas into a plasma has been observed. The time evolution of several quantities characterizing the state of the plasma, such as the plasma density [1, 2], the degree of ionization [4, 5, 6] or the energy-resolved atomic level population [3] have been measured using various plasma diagnostic methods.

These experiments, which have paved the way towards an unexplored regime of ionized gases, give rise to new phenomena in atomic physics as well as in plasma physics. Hence, a number of different theoretical approaches have been formulated to cover different aspects of these experiments [7, 8, 9, 10, 11, 12, 13].

An important issue is the question whether the plasma produced would be strongly coupled or not. The correlation strength is determined by the Coulomb coupling parameter  $\Gamma = e^2/(ak_{\rm B}T)$  with the Wigner-Seitz radius a [14]. A plasma is called "strongly coupled" if  $\Gamma \gg 1$ , i.e. if the Coulomb interaction between the plasma particles largely exceeds the thermal kinetic energy. In this case, interesting ordering effects such as Coulomb crystallization can be observed [15, 16]. For the initial conditions of the NIST experiments [1, 2, 3], however, the development of equilibrium electron-electron correlations leads to a rapid heating of the electron gas, which prevents the electron Coulomb coupling parameter  $\Gamma_{\rm e}$  from exceeding unity [7]. The same has been argued for an ion plasma in [17]. Since the electron dynamics proceeds on a much smaller timescale than the ion motion, in [7, 8] the electron heating could be studied for the early stage of the plasma evolution only, where the ionic component does not show dynamical effects. On the other hand, ion heating has only been studied in the framework of a model system, consisting of a homogeneous gas of Debye-screened ions [17], such that the influence of the subsequent expansion could not be explored.

The first quantitative comparison with experimental observations has been given in [10], with the plasma dynamics modeled within a hydrodynamical approach and ionization, excitation and recombination treated by a separate set of rate equations. Since this model does only account for the mean-field potential created by the charges, it cannot describe effects of particle correlations. However, it has also been shown there that the electronic Coulomb coupling parameter  $\Gamma_{\rm e}$  does not exceed a value of  $\approx 0.2$  during the plasma expansion due to heating by three-body recombination. Thus, the influence of electron-electron correlations on the dynamics of the plasma could be neglected. On the other hand, three-body recombination does not influence the ionic temperature, so that the ions can heat up only through correlation heating (and energy exchange with the electrons, which, however, is very slow). Since the ionic temperature was set to zero in [10], the role of ion-ion correlations could not be explored. In a preliminary study [13], we showed that they indeed change the evolution of the system quantitatively, though not qualitatively. In the following, we will give a detailed account of the kinetic model used in [13] and of all relevant ingredients. We will also develop a hybrid molecular dynamics (H-MD) approach which treats the electronic plasma component in an adiabatic approximation while the ions are fully accounted for. Such an approach permits the description of situations where the ions are strongly coupled [16, 18], which is clearly beyond the capabilities of the simple kinetic model. Nevertheless, for the typical situations realized in the experiments [1, 2, 3], comparison of the two theoretical approaches yields very good agreement, corroborating our findings reported earlier [13] and establishing firmly that one can capture the relevant physics with the relatively simple kinetic approach.

### II. THEORETICAL APPROACH

Our kinetic approach is similar to the one of [10]. The main difference is the inclusion of ion-ion correlations (IC) which will be described in detail below. Briefly, a set of kinetic equations is formulated for the evolution of the plasma (subsection II A), while ionization/excitation and recombination/deexcitation are taken into account on the basis of rate equations (subsection II B). In order to test the applicability and accuracy of this model, we have developed a less approximative and more flexible but computationally much more demanding approach. It uses molecular dynamics for the ionic motion while the electron component is treated as a fluid assuming a quasi-steady state (subsection II C).

# A. Kinetic description

Starting from the first equation of the BBGKY hierarchy, the evolution equation for the one-particle distribution function  $f_{\alpha}(\mathbf{r}, \mathbf{v}, t)$  of the free plasma charges is obtained as

$$m_{\alpha} (\partial_t + \mathbf{v}\partial_{\mathbf{r}}) f_{\alpha}(\mathbf{r}, \mathbf{v}, t) = \sum_{\beta} \int [\partial_{\mathbf{r}} \varphi_{\alpha\beta}(\mathbf{r}, \mathbf{r}')] \partial_{\mathbf{v}} f_{\alpha\beta}(\mathbf{r}, \mathbf{v}, \mathbf{r}', \mathbf{v}', t) d\mathbf{r}' d\mathbf{v}', \qquad (1)$$

where  $\alpha$ ,  $\beta$  label the particle species (e,i for electrons and ions, respectively),  $f_{\alpha\beta}(\mathbf{r}, \mathbf{v}, \mathbf{r}', \mathbf{v}', t)$  denotes the two-particle distribution function for the corresponding particle species and  $\varphi_{\alpha\beta} = q_{\alpha}q_{\beta}/|\mathbf{r} - \mathbf{r}'|$  is the Coulomb interaction potential between the charges  $q_{\alpha}$  and  $q_{\beta}$ . Electron-electron correlations are very small during the plasma expansion, since the electrons will quickly heat up due to three-body recombination and the additional heating due to correlation effects is small in comparison [10]. Hence, we neglect electron-electron as well as electron-ion correlations, leaving only IC as a possible influence on the plasma dynamics beyond the mean-field level. On this level of approximation the ion kinetic equation can be written as

$$m_{\rm i} \left( \partial_t + \mathbf{v} \partial_{\mathbf{r}} - \frac{\partial_{\mathbf{r}} \bar{\varphi}}{m_{\rm i}} \partial_{\mathbf{v}} \right) f_{\rm i} = \int \left( \partial_{\mathbf{r}} \varphi_{\rm ii} \right) \, \partial_{\mathbf{v}} w_{\rm ii}(\mathbf{r}, \mathbf{v}, \mathbf{r}', \mathbf{v}') \, d\mathbf{r}' d\mathbf{v}' \,, \tag{2}$$

where the function

$$w_{ii}(\mathbf{r}, \mathbf{v}, \mathbf{r}', \mathbf{v}') = f_{ii}(\mathbf{r}, \mathbf{v}, \mathbf{r}', \mathbf{v}') - f_{i}(\mathbf{r}, \mathbf{v}) f_{i}(\mathbf{r}', \mathbf{v}')$$
(3)

contains the contributions of IC to the two-particle distribution function and  $\bar{\varphi}$  is the meanfield potential created by all plasma charges. Since  $m_{\rm e}/m_{\rm i} \ll 1$ , the relaxation timescale of the electrons is much smaller than the timescale of the plasma expansion under typical experimental conditions [1]. Thus, we may safely apply an adiabatic approximation for the electron distribution function, assuming a local Maxwellian distribution

$$f_e(\mathbf{r}, \mathbf{v}) \propto \exp\left(\frac{\bar{\varphi}(\mathbf{r})}{k_{\rm B}T_{\rm e}}\right) \exp\left(-\frac{\mathbf{v}^2}{2k_{\rm B}T_{\rm e}}\right) ,$$
 (4)

where  $T_{\rm e}$  is the electron temperature. Eq. (4) together with a quasineutral approximation [19] allows one to express the mean-field potential in terms of the ionic density  $\rho_{\rm i} = \int f_{\rm i} d{\bf v}$ , resulting in

$$\partial_{\mathbf{r}}\bar{\varphi} = k_{\rm B}T_{\rm e}\frac{\partial_{\mathbf{r}}\rho_{\rm i}}{\rho_{\rm i}} \ . \tag{5}$$

Using Eq. (5), the following evolution equations for the second moments of the ion distribution function are derived from Eq. (2)

$$\partial_t \langle r^2 \rangle = 2 \langle \mathbf{r} \mathbf{v} \rangle$$
 (6a)

$$\frac{m_{\rm i}}{2}\partial_t \langle \mathbf{r}\mathbf{v} \rangle = \frac{m_{\rm i}}{2} \langle v^2 \rangle + \frac{3}{2}k_{\rm B}T_{\rm e} + \frac{1}{2}N_{\rm i}^{-1} \int \rho_{\rm i}(\mathbf{r})\mathbf{r}\mathbf{F}_{\rm ii}(\mathbf{r}) d\mathbf{r}$$
(6b)

$$\frac{m_{\rm i}}{2} \partial_t \left\langle v^2 \right\rangle = N_{\rm i}^{-1} \left( k_{\rm B} T_{\rm e} \int \rho_{\rm i} \partial_{\rm r} \mathbf{u} \, d\mathbf{r} - \int \mathbf{v} (\partial_{\mathbf{r}} \varphi_{\rm ii}) w_{\rm ii}(\mathbf{r}, \mathbf{v}, \mathbf{r}', \mathbf{v}') \, d\mathbf{r} d\mathbf{v} d\mathbf{r}' d\mathbf{v}' \right)$$
(6c)

where  $\langle r^2 \rangle = N_{\rm i}^{-1} \int r^2 f_{\rm i}({\bf r},{\bf v}) d{\bf r} d{\bf v}$  etc. The "correlation force"  ${\bf F}_{\rm ii}({\bf r})$  is given by

$$\mathbf{F}_{ii}(\mathbf{r}) = -\int \left(\partial_{\mathbf{r}}\varphi_{ii}\right)\rho_{i}(\mathbf{r}')g_{ii}(\mathbf{r},\mathbf{r}')\,d\mathbf{r}'\,,\tag{7}$$

where the spatial correlation function  $g_{ii}$  is defined by  $\rho_i(\mathbf{r})\rho_i(\mathbf{r}')g_{ii}(\mathbf{r},\mathbf{r}') \equiv \int w_{ii}(\mathbf{r},\mathbf{v},\mathbf{r}',\mathbf{v}') d\mathbf{v}d\mathbf{v}'$  and  $\mathbf{u}(\mathbf{r}) = \int \mathbf{v}f_i d\mathbf{v}$  is the hydrodynamical drift velocity of the plasma. With the help of the second kinetic ion equation of the BBGKY hierarchy, the last term on the right-hand side of Eq. (6c) can be written as

$$\frac{1}{N_{i}} \int \mathbf{v}(\partial_{\mathbf{r}}\varphi_{ii}) w_{ii} d\mathbf{r} d\mathbf{v} d\mathbf{r}' d\mathbf{v}' = -\frac{1}{2N_{i}} \partial_{t} \int \varphi_{ii} w_{ii} d\mathbf{r} d\mathbf{v} d\mathbf{r}' d\mathbf{v}'$$

$$= -\partial_{t} U_{ii} , \qquad (8)$$

where

$$U_{ii} = \frac{1}{2N_i} \int \varphi_{ii} \rho_i(\mathbf{r}) \rho_i(\mathbf{r}') g_{ii}(\mathbf{r}, \mathbf{r}') d\mathbf{r} d\mathbf{r}'$$
(9)

is the average correlation energy per ion. Hence, Eq. (6c) reflects energy conservation for the ion subsystem. The evolution of the hydrodynamical velocity  $\mathbf{u}$  is determined by

$$m_{\rm i}\rho_{\rm i} \left[\partial_t \mathbf{u} + (\mathbf{u} \cdot \partial_{\mathbf{r}}) \mathbf{u}\right] = -k_{\rm B}T_{\rm e}\partial_{\mathbf{r}}\rho_{\rm i} - \partial_{\mathbf{r}}P_{\rm th,i} - \rho_{\rm i}\mathbf{F}_{\rm ii}$$
 (10)

where  $P_{\text{th,i}} = \frac{m_i}{3N_i} \int (\mathbf{v} - \mathbf{u})^2 f_i d\mathbf{r} d\mathbf{v}$  is the thermal ion pressure. As shown in the appendix, in the framework of a local density approximation, i.e. by assuming that  $g_{ii}$  only depends on the distance  $|\mathbf{r} - \mathbf{r}'|$  and on the densities at the two coordinates  $\mathbf{r}$  and  $\mathbf{r}'$ , and that the ionic density  $\rho_i$  varies slowly on the lengthscale where g is significantly different from zero, the total correlation energy can be approximated by the well-known LDA expression

$$U_{ii} = N_i^{-1} \int u_{ii} \rho_i \, d\mathbf{r} \tag{11}$$

while the correlation force is found to be

$$\mathbf{F}_{ii} = -\frac{1}{3} \left( \frac{u_{ii}}{\rho_i} + \frac{\partial u_{ii}}{\partial \rho_i} \right) \partial_{\mathbf{r}} \rho_i \quad , \tag{12}$$

where  $u_{ii}(\mathbf{r})$  is the correlation energy of a homogeneous plasma of density  $\rho_i(\mathbf{r})$ ,

$$u_{ii}(\mathbf{r}) = \frac{e^2}{2} \rho_i(\mathbf{r}) \int \frac{g_{ii}(x; \rho_i)}{x} d\mathbf{x} . \tag{13}$$

If IC are neglected in Eq. (2), the kinetic equation exhibits the following selfsimilar solution

$$f_{\rm i} \propto \exp\left(-\frac{r^2}{2\sigma^2}\right) \exp\left(-\frac{m_{\rm i} \left(\mathbf{v} - \mathbf{u}\right)^2}{2k_{\rm B}T_{\rm i}}\right)$$
  
 $\mathbf{u} = \gamma \mathbf{r}$  (14)

which corresponds to the initial state of the experiments under consideration. As soon as IC are taken into account via the correlation pressure  $\rho_i \mathbf{F}_{ii}$  in Eq. (10), however, Eqs. (14) are no longer exact solutions of Eq. (2). Using Eq. (12), the last term on the right-hand side of Eq. (10) can be rewritten as  $\rho_i \mathbf{F}_{ii} = -\frac{1}{3} \frac{\partial (u_{ii} \rho_i)}{\partial \rho_i} \partial_{\mathbf{r}} \rho_i$ . Interpreting this term as a local nonideal pressure, an equation for the parameter  $\gamma$  was derived in [13] by averaging the differential equation for  $|\mathbf{u}|/r$  obtained by inserting Eq. (14) into Eq. (10) over the plasma volume. Obviously, this treatment is not unique. Since, as discussed above, the ansatz (14) does not solve Eq. (10) exactly, multiplying Eq. (10) by different functions of r and averaging over the plasma volume will lead to slightly different evolution equations for the parameter  $\gamma$ . Here, supported by a comparison with our numerical results from the MD simulations, to be discussed below, we assume as in [13] that the functional form of the hydrodynamical quantities of Eqs. (14) is not altered by the inclusion of IC, while the dynamics of the parameters appearing in Eqs. (14) is determined from the equations (6) for the moments of the distribution function. Clearly, such an approximation can not be a priori justified. Hence, it must be validated a posteriori by comparison with more sophisticated methods which do not rely on a reduction of the plasma description to a few macroscopic parameters.

With this procedure, we arrive at the following set of equations for the width  $\sigma$  of the plasma cloud, its expansion velocity  $\gamma \mathbf{r}$  as well as ionic and electronic temperature  $T_i$  and  $T_e$ :

$$\partial_t \sigma^2 = 2\gamma \sigma^2 \tag{15a}$$

$$\partial_t \gamma = \frac{k_{\rm B} T_{\rm e} + k_{\rm B} T_{\rm i} + \frac{1}{3} U_{\rm ii}}{m_{\rm i} \sigma^2} - \gamma^2 \tag{15b}$$

$$\partial_t k_{\rm B} T_{\rm i} = -2\gamma k_{\rm B} T_{\rm i} - \frac{2}{3} \gamma U_{\rm ii} - \frac{2}{3} \partial_t U_{\rm ii}$$
 (15c)

$$\partial_t k_{\rm B} T_{\rm e} = -2\gamma k_{\rm B} T_{\rm e} . \tag{15d}$$

The last equation (15d) has been derived from the electron kinetic equation by making use of the quasineutrality condition. The set of Eqs. (15) slightly differs from that presented in [13] where  $W_{\rm c} = \frac{1}{3N_{\rm i}} \int \rho_{\rm i} \frac{\partial (u_{\rm ii}\rho_{\rm i})}{\partial \rho_{\rm i}} d{\bf r}$  had been used instead of  $U_{\rm ii}$  in Eq. (15b). A comparison with our numerical MD results shows that Eqs. (15) yield a slightly better quantitative agreement, while the principal influence of IC on the plasma dynamics, which has been partly discussed in [13], is the same. Eqs. (15) provide a transparent physical picture of the expansion dynamics. First, Eq. (15d) together with (15a) reflects the adiabatic cooling of the electron gas, i.e.  $T_e \sigma^2 = \text{const.}$  The ion temperature, on the other hand, is not only affected by the adiabatic cooling, expressed by the first term in Eq. (15c), but also changes due to the development of IC, which is taken into account by the last term in Eq. (15c). Furthermore, these correlations reduce the ion-ion interaction and therefore lead to an effective negative acceleration, expressed by the  $U_{ii}/3$ -term in Eq. (15b), in addition to the ideal thermal pressure. This contribution, which corresponds to the average nonideal pressure known from homogeneous systems [14, 15], also leads to an effective potential in which the ions move. As they expand in this potential, the thermal energy changes due to energy conservation, as expressed by the second term on the right-hand side of Eq. (15c). Finally, combining eqs. (15) yields a second integral of motion, namely the total energy of the plasma

$$E_{\text{tot}} = \frac{3}{2} \left( k_{\text{B}} T_{\text{e}} + k_{\text{B}} T_{\text{i}} \right) + \frac{3}{2} m_{\text{i}} \gamma^2 \sigma^2 + U_{\text{ii}} . \tag{16}$$

Although the set of equations (15) determines the time evolution of all relevant macroscopic plasma parameters, namely its width, expansion velocity, electron and ion temperature, it is not a closed set since an evolution equation for the correlation energy  $U_{ii}$  which enters Eq. (15c) is missing. Initially, the plasma is completely uncorrelated, so that  $U_{ii}(t=0)=0$ . However, the initial state corresponds to a non-equilibrium situation, and the plasma will relax towards thermodynamic equilibrium, thereby building up correlations. A precise description of this relaxation process in the framework of a kinetic theory is rather complicated and requires a considerable numerical effort [20]. We therefore employ a linear approximation for the relaxation of the two-particle correlation function, the so-called correlation-time approximation [21],

$$\frac{dw_{ii}(\mathbf{r}, \mathbf{v}, \mathbf{r}', \mathbf{v}'; t)}{dt} \approx -\frac{w_{ii}(\mathbf{r}, \mathbf{v}, \mathbf{r}', \mathbf{v}'; t) - w_{ii}^{eq}(\mathbf{r}, \mathbf{r}'; t)}{\tau_{corr}}.$$
(17)

Here,  $\tau_{\rm corr}$  [21, 22] is the characteristic timescale for the relaxation of particle correlations and

 $w_{ii}^{\text{eq}}$  is the equilibrium pair correlation function, which in our case still depends on time via the evolving one-particle distribution function since the plasma is freely expanding. As shown in [23] the correlation time  $\tau_{\text{corr}}$  can be well estimated by the inverse ionic plasma frequency. Hence, in our calculations we set  $\tau_{\text{corr}} = \omega_{\text{p,i}}^{-1} = \sqrt{m_{\text{i}}/(4\pi e^2 \bar{\rho}_{\text{i}})}$ , where  $\bar{\rho}_{\text{i}} = N_{\text{i}}/(4\pi\sigma^2)^{3/2}$  is the average ionic density of the plasma. Such a linear approximation is good only for small deviations of  $w_{\text{ii}}$  from its equilibrium form. Clearly, this is not the case in the initial stage of the gas evolution. However, after the initial phase of correlation heating the system stays very close to its slowly changing local equilibrium, and one may expect Eq. (17) to yield good results. Under the same conditions that lead to Eqs. (11) and (12), one easily verifies that Eq. (17) leads to

$$\partial_t U_{\rm ii} \approx -\frac{U_{\rm ii} - U_{\rm ii}^{\rm eq}}{\tau_{\rm corr}},$$
 (18)

where  $U_{ii}^{eq} = N_i^{-1} \int \rho_i u_{ii}^{eq} d\mathbf{r}$  and  $u_{ii}^{eq}(\mathbf{r})$  is the correlation energy per particle of a homogeneous one-component plasma in local equilibrium. This quantity has been studied intensively in the past, and approximate analytical formulae are available in the literature [14, 15]. Here, we adopt the interpolation formula from [24]

$$u_{\rm ii}^{\rm eq}(\mathbf{r}) = k_{\rm B} T_{\rm i} \Gamma^{3/2} \left( \frac{A_1}{\sqrt{A_2 + \Gamma}} + \frac{A_3}{1 + \Gamma} \right) , \qquad (19)$$

with  $A_1 = -0.9052$ ,  $A_2 = 0.6322$  and  $A_3 = -\sqrt{3}/2 - A_1/\sqrt{A_2}$ , which yields an accurate interpolation between the low- $\Gamma$  Abe limit and the high- $\Gamma$  behavior obtained by Monte Carlo and MD simulations. It should be noted that in the present situation  $u_{ii}$  depends on time since the plasma expands. Hence,  $\Gamma$  and with it the thermodynamical equilibrium change in time.

The set of equations (15) describes the evolution of the plasma part of the system, i.e. a system of  $N_i$  ions and electrons. Due to ionization and recombination events occurring during the plasma expansion (discussed in detail in the following subsection), this number  $N_i$ , and hence also the total mass  $M = N_i m_{\text{atom}}$ , is not constant over the course of the evolution. However, such a treatment completely neglects the influence of the bound Rydberg atoms on the dynamics. One may argue that they do not influence the plasma evolution since they do not interact with the ions or electrons by Coulomb interaction. On the other hand, a Rydberg atom may carry a significant amount of kinetic energy, gained from the acceleration by the electron pressure before its formation by three-body recombination. In a simple approximation, we assume equal hydrodynamical velocities and density profiles for

the ions and atoms, in order to account for this effect. This implies that the expansion of the neutral Rydberg atoms can be taken into account by replacing the mass  $N_i m_i$  of the ions by the mass of the *total* system  $(N_i + N_a)m_i$ , where  $N_a$  is the number of atoms. We therefore replace the ion mass  $m_i$  by an effective mass  $(1 + N_a/N_i)m_i$  in Eq. (15b). The quality of this approximation can, of course, also be checked by comparison with the H-MD description, see below.

### B. Ionization and Recombination

As demonstrated in [10], a satisfactory description of the dynamics of an ultracold plasma can be achieved by combining a hydrodynamic treatment of the plasma evolution with rate equations accounting for inelastic collisions between the plasma particles and Rydberg atoms. The rate equation for the change of density of Rydberg atoms in a state with principal quantum number n reads

$$\dot{\rho}_{a}(n) = \rho_{e} \sum_{p} \left[ K(p, n) \rho_{a}(p) - K(n, p) \rho_{a}(n) \right] + \rho_{e} \left[ R(n) \rho_{e} \rho_{i} - I(n) \rho_{a}(n) \right] , \qquad (20)$$

where K(p, n) is the rate coefficient for electron impact (de)excitation from level p to level n, and R(n) and I(n) describe three-body recombination into and electron-impact ionization from level n, respectively. The rate coefficients K, R and I have been taken from the classic work of Mansbach and Keck [25]. Additional processes, such as, e.g., ionization by black-body radiation or from dipolar atom-atom interactions, are easily included in Eq. (20) if the corresponding rates are available. Such processes are essential for a description of the early stages of the evolution of a system starting with a Rydberg gas [4, 5, 6], but are of minor importance in situations starting from a pure plasma.

In this framework, the evolution of the system is obtained by solving Eqs. (15a)-(15c) together with Eq. (20) while the electron temperature is now obtained from the modified energy conservation relation  $E_{\text{tot}} + E_{\text{a}} = \text{const.}$  instead of Eq. (15d), where  $E_{\text{a}} = -\mathcal{R} \sum_{n} N_{\text{a}} n^{-2}$  is the total energy of the Rydberg atoms and  $\mathcal{R} = 13.6 \text{ eV}$ .

### C. Hybrid molecular dynamics treatment

As we will show in section III, the kinetic description of the previous subsections is able to describe the plasma dynamics to a surprisingly large extent. However, one of the main motivations of this work is the study of the role of IC, which are incorporated in the model only in an approximate way. To assess their influence on the dynamics reliably, a more sophisticated approach is required, e.g. molecular dynamics simulations which fully incorporate the ionic interactions. However, a full MD simulation of both, electrons and ions, is computationally very demanding, and only the very early stage of the system evolution can be described in this way [7]. On the other hand, as argued above, electronic correlations are not important for the plasma dynamics, so that only IC have to be accounted for in full while the influence of the electrons on the dynamics may be treated on a mean-field level. Moreover, we have seen that the timescale of equilibration of the electronic subsystem is orders of magnitude shorter than that of the ionic subsystem and the timescale of the plasma expansion. This observation led us to use an adiabatic approximation in subsection II A, where the electrons are assumed to equilibrate instantaneously, assuming a Maxwellian velocity distribution with a well-defined temperature and a spatial profile determined from the total mean-field potential of the plasma charges. The clear separation of timescales suggests that this adiabatic approximation is well justified, hence we will keep it in the following. Consequently, we have developed a hybrid approach where the electrons are treated on a hydrodynamical level as in the kinetic description above, while the ions are propagated individually with their mutual interaction and the influence of the electrons on the ions enters via the electronic mean-field potential. This hybrid approach permits the use of much larger timesteps in the propagation of the system, since the electronic dynamics needs not to be followed in detail but only the ionic motion has to be resolved in time. Consequently, the evolution of the system can be followed over the experimental timescales. Furthermore, the approximate treatment of IC in the kinetic model of subsection II A can be tested. Finally, beyond the scope of the present work, we have shown [16] that the present H-MD approach can describe situations where the ionic plasma component is so strongly coupled that crystallization of the ions sets in. Such a scenario is clearly beyond the capabilities of a kinetic approach.

As discussed above, the electrons are still treated as a fluid, while we lift the quasineutral

approximation by calculating the resulting mean-field potential from the Poisson equation

$$\Delta \bar{\varphi} = 4\pi e^2 \left( \rho_{\rm e} - \rho_{\rm i} \right). \tag{21}$$

However, using Eq. (4) poses a conceptual difficulty [11] since the mean-field potential approaches a finite value at large distances and therefore leads to a non-normalizable electron density. This problem, which has been discussed for a long time in an astrophysical context [26], reflects the fact that a substantial fraction of the electrons indeed escapes the finite potential barrier at long times during the relaxation process until the total kinetic energy of all electrons is less than the height of the potential well. On the timescales under consideration, however, typically only a small amount of the electrons escapes the plasma volume, until the resulting charge imbalance becomes large enough to trap the remaining electrons, which quickly reach a quasi-steady state forming a temporarily quasineutral plasma in the central region. We account for this electron loss by determining the fraction of trapped electrons from the results of Ref. [1].

The corresponding steady-state distribution, derived for the study of globular clusters, is of the form [27]

$$\rho_{\rm e} \propto \exp\left(\frac{\bar{\varphi}}{k_{\rm B}T_{\rm e}}\right) \int_0^{\chi} \exp\left(-x\right) x^{3/2} dx,$$
(22)

where  $\chi = m_{\rm e}v_{\rm esc}^2/(2k_{\rm B}T_{\rm e})$  with the velocity  $v_{\rm esc}(\mathbf{r})$  necessary to escape from a given position in the plasma. In the present case, the potential can have a non-monotonous radial space dependence and the escape velocity has to be defined as

$$\frac{m_{\rm e}}{2}v_{\rm esc}^{2}\left(r\right) = \max_{r'>r} \left[\bar{\varphi}\left(r'\right) - \bar{\varphi}\left(r\right)\right],\tag{23}$$

in contrast to astrophysical problems where one only has a single sign of "charge" and  $m_{\rm e}v_{\rm esc}^2/2 = -\bar{\varphi}$  [27]. For a given electron temperature  $T_{\rm e}$  and ion density  $\rho_{\rm i}$  the electron density is found by numerical iteration of Eqs. (21), (22) and (23) until selfconsistency is reached.

Knowledge of the electron density then permits propagation of the ions in the electron mean-field  $\Delta \bar{\varphi}_{\rm e} = 4\pi e^2 \rho_{\rm e}$  and the full interaction potential of the remaining ions,

$$m_{i}\ddot{\mathbf{r}}_{j} = \partial_{\mathbf{r}_{j}}\bar{\varphi}_{e} + e^{2} \sum_{k} \frac{\mathbf{r}_{j} - \mathbf{r}_{k}}{\left|\mathbf{r}_{j} - \mathbf{r}_{k}\right|^{3}}.$$
 (24)

The numerical solution of the ion equations of motion represents the most time consuming part of the plasma propagation. In general, for N propagated particles, the corresponding

numerical effort scales with  $N^2$  rendering a treatment of large particle numbers difficult. In order to simulate particle numbers relevant to the experiments, we have adapted a hierarchical treecode originally designed for astrophysical problems, first described in [28]. This method provides a numerically exact solution of the ion equations of motion Eq. (24), while the numerical effort grows only as  $N \ln N$  with increasing N. More details about the numerical procedure can be found, e.g., in [29].

In the framework of the kinetic model introduced in section II A, the influence of IC on the system evolution can be singled out by comparison with the solution of the corresponding equations with  $U_{ii} \equiv 0$ . In order to make an analogous comparison also for the MD simulations, we have performed calculations propagating the ions in the mean-field potential created by all charges. Technically, the mean-field potential is represented using a test-particle method, widely used for various problems in plasma physics (see, e.g., [30]).

### III. RESULTS AND DISCUSSION

We will discuss the evolution of a plasma initially consisting of  $N_{\rm e}=37500$  electrons and  $N_{\rm i}=40000$  ions with an average density of  $10^9~{\rm cm}^{-3}$  at a rather low electronic kinetic energy  $E_{\rm e}=3k_{\rm B}T_{\rm e}/2=20$  K, comparing the results from the kinetic model and our MD simulation. Thereby, we put special emphasis on the role of IC.

### A. Global aspects of plasma expansion and recombination

The general macroscopic behavior of the system has been described before in several publications, experimentally as well as theoretically [2, 3, 10, 11]. The plasma cloud slowly expands due to the thermal pressure of the electrons, leading to adiabatic cooling of the electrons as well as partial recombination into bound states (figures 1 and 2). The amount of recombination and its influence strongly depends on the initial electron temperature and density. If the electrons are too hot (about 50 K for typical experimental densities of 10<sup>9</sup> cm<sup>-3</sup>), recombination is strongly suppressed and the system dynamics is well described by the results of [19] obtained for the collisionless plasma expansion [2].

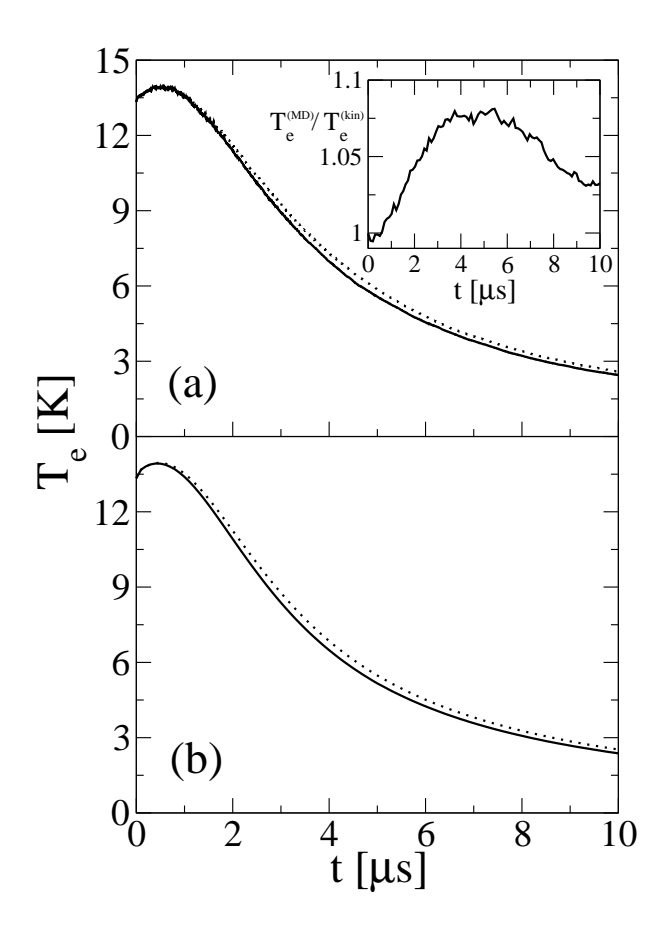


FIG. 1: Electronic temperature  $T_{\rm e}(t)$  for an expanding plasma of 40000 ions with an initial average density of  $10^9 {\rm cm}^{-3}$  and an initial electron kinetic energy of 20 K, obtained from the H-MD simulation (a) and the kinetic model (b), with (solid) and without (dotted) the inclusion of IC. The inset shows the ratio of the electron temperatures obtained from the H-MD simulation and the kinetic model.

# 1. Temporal evolution of the electronic temperature

For the lower electron temperatures considered here, as can be seen in Fig. 1, there is an initial increase of the electron temperature due to electron heating by three-body recombination and subsequent deexcitation of the formed Rydberg atoms. At low initial electron energies this heating drastically increases the electron temperature and thus accelerates the plasma expansion [10], which explains the enhanced expansion velocity observed in [2]. In contrast to this recombination heating of the electrons, the inclusion of IC only slightly changes the expansion dynamics, as seen in Fig. 1 by comparing the solid and dotted lines. As shown in the inset of Fig. 1a, the electron temperature obtained from the H-MD sim-

ulation and the kinetic model differ by at most 8% during the first few microseconds of the plasma expansion, while the agreement becomes even better at later times. Moreover, the faster decrease of the electron temperature due to the inclusion of IC, predicted by the particle simulations, is quantitatively reproduced by the much simpler kinetic model.

Hence, the simple evolution equations (15) are sufficient to clarify the role of IC in the expansion dynamics. According to Eq. (15c), the development of IC quickly heats up the plasma ions to roughly  $-\frac{2}{3}U_{ii}$  since the expansion of the plasma is still negligible during this initial stage. Thereby, the negative correlation energy term  $\frac{1}{3}U_{ii}$  in Eq. (15b) is overcompensated, leading to a faster expansion of the plasma. As a consequence of the quicker expansion, the electron temperature decreases somewhat faster than without the inclusion of IC. With Eq. (15b), the importance of this effect can be estimated by comparing the thermal electron energy  $k_{\rm B}T_{\rm e}$  to the net ion contribution  $-\frac{1}{3}U_{ii}$  in the numerator of the first term on the right-hand side of Eq. (15b). Estimating the correlation energy by  $e^2/a$ , it follows that the total pressure driving the plasma expansion is enhanced by a factor of roughly  $1 + \Gamma_{\rm e}/3$ , which only slightly changes the expansion dynamics since the electrons are known to be weakly coupled over the whole observation time [10].

# 2. Formation of Rydberg atoms in time

The number of recombined atoms is influenced more strongly by IC (Fig. 2). During the evolution of the system, Rydberg atoms are constantly formed by three-body recombination and re-ionized by the free electrons in the plasma. As shown in Fig. 2a, for the current set of parameters about 7000 Rydberg atoms are present in the system after 40  $\mu$ s, while the kinetic model yields about 7900 atoms at the same instant of time (Fig. 2b). This number is small compared to the size of the whole system, nevertheless it is large enough that the recombined atoms can be detected in an experiment, and corresponding curves have indeed been obtained experimentally [3]. Due to the strong temperature dependence of the total three-body recombination rate, which is proportional to  $T_e^{-9/2}$  [25], the slight decrease of the electron temperature due to the faster expansion, caused by the correlation heating of the ions, considerably affects the recombination behavior of the plasma. While there is an overall shift between the atom number obtained from the particle simulations and the kinetic model, both the kinetic model and the H-MD simulation yield an increase of the

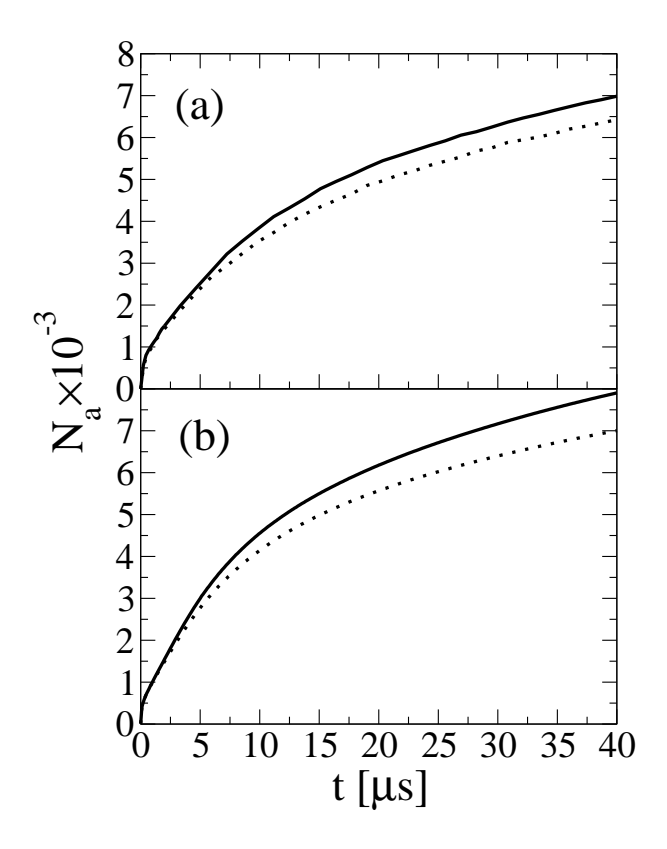


FIG. 2: Number  $N_a(t)$  of recombined atoms obtained from the H-MD simulation (a) and the kinetic model (b) for the same parameters as in Fig. 1. The solid line shows the result taking into account the IC while the dotted line is obtained from the mean-field treatment.

atom number of about 10% at  $t = 40 \,\mu\text{s}$  (Fig. 2), compared to a mean-field treatment of the ion dynamics. Thus, the H-MD simulation corroborates our previous findings [13].

Additional insight into the recombination process can be gained from a closer look at the distribution of bound Rydberg states. Figure 3 shows the population of levels with principal quantum number n for three different times, corresponding to different stages of the plasma expansion. Initially, Rydberg states of moderate excitation are populated, due to a relatively high electron temperature (Fig. 3a). At later times, higher excited bound states are formed in the course of the plasma expansion (Figs. 3b and 3c), since the maximum principal quantum number for recombination  $n_{\text{max}} = \sqrt{\mathcal{R}/(2k_{\text{B}}T_{\text{e}})}$  [25] increases as the electron temperature drops down. Moreover, the deeply bound states formed at earlier times are also not subject to electron-impact excitation and deexcitation anymore since the thermal velocity of the impacting electrons has become too small. Thus, as becomes apparent by comparing Fig. 3b with 3c, the deeply bound states ( $n \lesssim 30$ ) remain basically untouched, while higher and

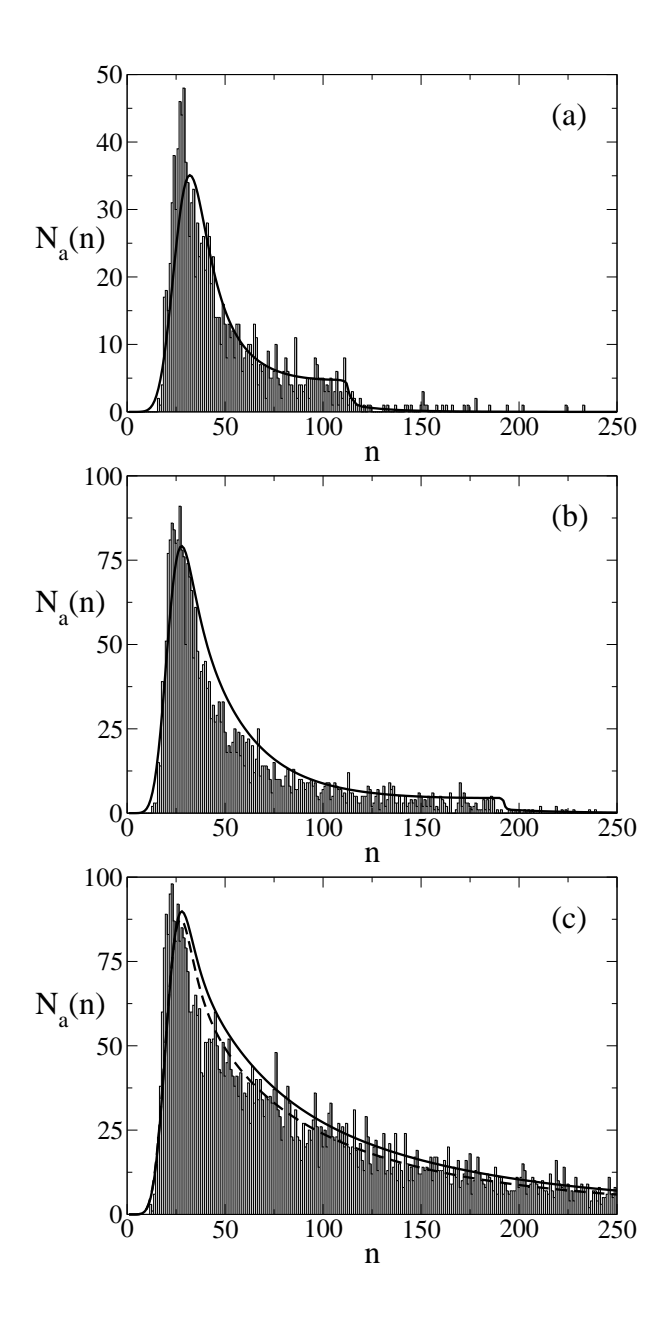


FIG. 3: Population of bound Rydberg states with principal quantum number n, after  $t = 1.5 \,\mu\text{s}$  (a),  $t = 6 \,\mu\text{s}$  (b) and  $t = 40 \,\mu\text{s}$  (c). The vertical bars represent the H-MD calculation, the solid line the kinetic model. The dashed curve in (c) shows the kinetic model neglecting IC. Initial-state parameters are the same as in Fig. 1.

higher states "freeze out" as the plasma expands. As may be anticipated from Fig. 2, IC mainly affect the later stages of the plasma evolution. Hence, the inclusion of IC alters the population of these higher lying states, as shown in Fig. 3c. Since these states have small binding energy, they contribute little to the total kinetic energy of the plasma subsystem.

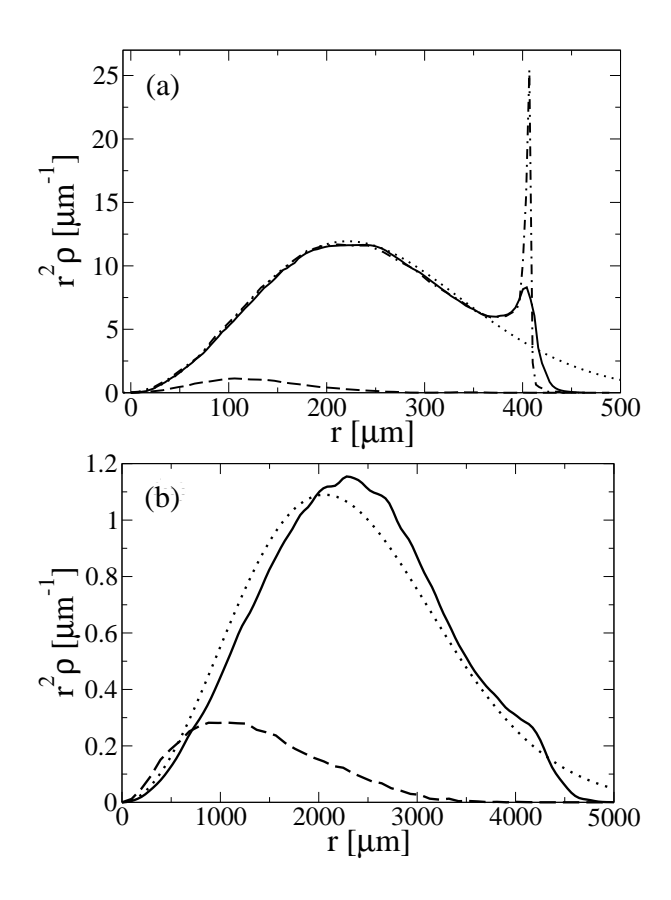


FIG. 4: Spatial densities  $\rho_i$  (solid) and  $\rho_a$  (dashed) of the ions and atoms, respectively, at  $t = 3 \,\mu s$  (a) and  $t = 31.3 \,\mu s$  (b), compared to the Gaussian profile assumed for the kinetic model (dotted). Additionally,  $\rho_i$  obtained from the particle simulation using the mean-field interaction only is shown as the dot-dashed line in (a). Initial-state parameters are the same as in Fig. 1.

This is the reason why the effect of IC is visible in the distribution of Rydberg states, but not in the macroscopic expansion dynamics of the plasma, reflected, e.g., by the asymptotic expansion velocity measured in [2].

# B. Spatially resolved plasma expansion and relaxation

While the time evolution of global, i.e. space-averaged, observables of the plasma is very well described by the kinetic model, one may expect discrepancies compared to the MD simulations when looking into the spatially resolved plasma dynamics. We will assess these discrepancies quantitatively in the following.

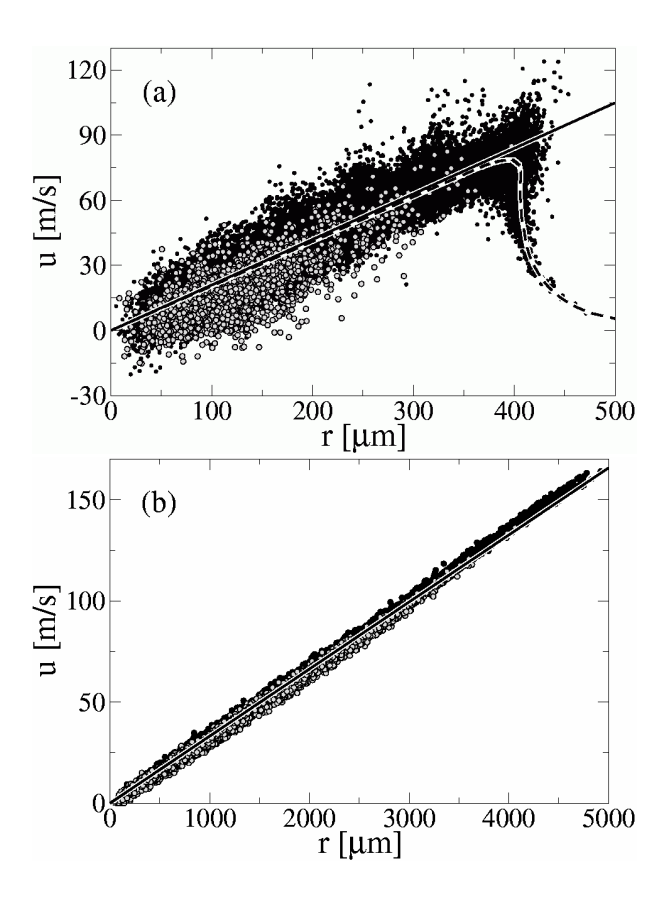


FIG. 5: Hydrodynamic velocity u(r) of ions (full circles) and atoms (open circles) at the same times as in Fig. 4, compared to the straight-line assumption of the kinetic model. The dashed line in (a) shows the result of the particle simulation using a mean-field treatment of the ion-ion interaction.

### 1. Evolution of the particle densities

In the derivation of the kinetic equations (15), we have assumed that the analytical form of the ionic density  $\rho_i$  remains invariant during the evolution of the system and, moreover, that the atoms will have the same distribution. As the plasma expands, the spatial profile of the ions must deviate from its original Gaussian shape [11]. This is mainly due to deviations from quasineutrality, e.g. deviations from the linear space dependence of the outward directed acceleration, at the plasma edge. The influence of the nonlinear correlation pressure on the density profile is of minor importance, as can be seen by comparing the solid and dot-dashed line of Fig. 4a in the inner plasma region. As known from earlier studies of expanding plasmas, based on a mean-field treatment of the particle interactions [11, 31, 32], a sharp spike develops at the plasma edge, shown by the dot-dashed line in Fig. 4a. At later times,

this spike decays again when the maximum of the hydrodynamic ion velocity passes the position of the density peak, so that the region of the peak is depleted. Ultimately, at long times, the plasma approaches a quasineutral selfsimilar expansion [32]. From Fig. 4a it becomes apparent that with IC the peak structure is less pronounced than in mean-field approximation. This is due to dissipation caused by ion-ion collisions which are fully taken into account in the H-MD simulation. As shown in [32], by adding an ion viscosity term to the hydrodynamic equations of motion, dissipation tends to stabilize the ion density and prevents the occurrence of wavebreaking which was found to be responsible for the diverging ion density at the plasma edge in the case of a dissipationless plasma expansion. Furthermore, the initial correlation heating of the ions largely increases the thermal ion velocities leading to a broadening of the peak structure compared to the zero-temperature case.

Apart from the deviations at the plasma edge, the ionic density is rather well reproduced by the Gaussian approximation for the spatial distribution. In particular, there is good agreement between the rms-radii obtained from the MD simulation and the kinetic model. On the other hand, the spatial distribution of atoms significantly deviates from that of the ions even at relatively early times due to the nonlinear density dependence of the collision rates in Eq. (20). However, as also stated in [11], the total number of atoms is too small to significantly influence the macroscopic expansion of the system.

# 2. Spatial dependence of the radial velocities

Another assumption used in the derivation of the kinetic model is the proportionality of the hydrodynamical expansion velocity to the distance from the center of the plasma cloud,  $\mathbf{u} = \gamma \mathbf{r}$ , both for the ions and the atoms. In order to check this assumption, we have calculated the radial velocity component  $v_r = \mathbf{vr}/r$  of each particle, which is plotted as a function of the radial distance from the plasma center in Fig. 5. At an early time the velocity distribution is spread out about its mean value predicted from the kinetic approach due to the finite ionic temperature. Note that the expansion is slower near the plasma edge due to the deviation from quasineutrality as discussed above. Consequently, the inner part of the plasma which expands more quickly will catch up with the outer rim, leading to the formation of the density spike seen in Fig. 4a. In the case of the H-MD simulation the velocity spread,

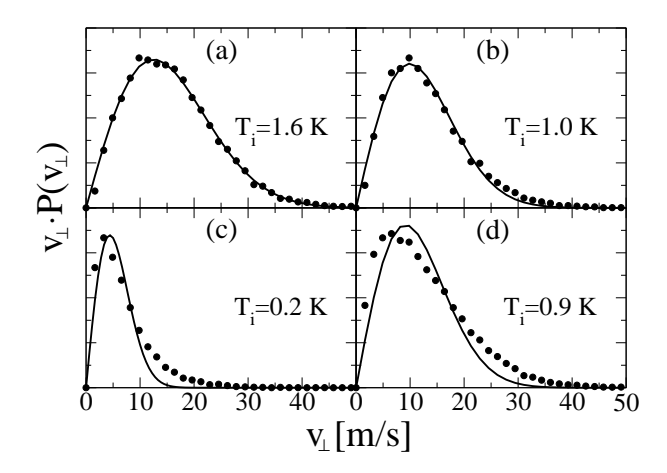


FIG. 6: Distribution of thermal ionic velocities at  $t = 0.3 \,\mu\text{s}$  sampled from three different regions of the plasma:  $r \leq 1.3\sigma$  (a),  $1.3\sigma < r \leq 2\sigma$  (b), and  $r > 2\sigma$  (c), and from the total plasma volume (d). The solid lines show a fit to a Maxwell-Boltzmann distribution corresponding to the temperatures specified in the figure. Initial-state parameters are the same as in Fig. 1.

caused by the initial ion heating, is of the same order of magnitude as the hydrodynamical expansion velocity itself, leading to a significant broadening of the density spike as discussed above. At later stages of the system evolution, the ions cool adiabatically due to the plasma expansion, and the width of the velocity distribution decreases significantly. Moreover, as discussed in connection with the decay of the ion density peak in Fig. 4b, the decrease of the ion velocities near the plasma edge apparent at early times has disappeared.

A comparison with the result of the kinetic model equations (15) shows once more that the H-MD simulation not only reproduces the linear radial dependence of the hydrodynamical velocity, but also yields a quantitative agreement between both methods.

# 3. Spatial dependence of the thermal velocities

Due to its marginal influence on the plasma expansion dynamics, the role of the ionic temperature  $T_i$  for the state of the system has not been addressed before. In the cold fluid model of [10, 11],  $T_i$  has been set to zero in order to follow the long-time plasma dynamics. However, as stated in the introduction, one of the motivations of the current type of experiments was the creation of a strongly coupled plasma. In this context, knowledge of  $T_i$  is essential since it directly enters the Coulomb coupling parameter which determines the state of the plasma. Moreover, the ionic temperature gives important insight into the relaxation

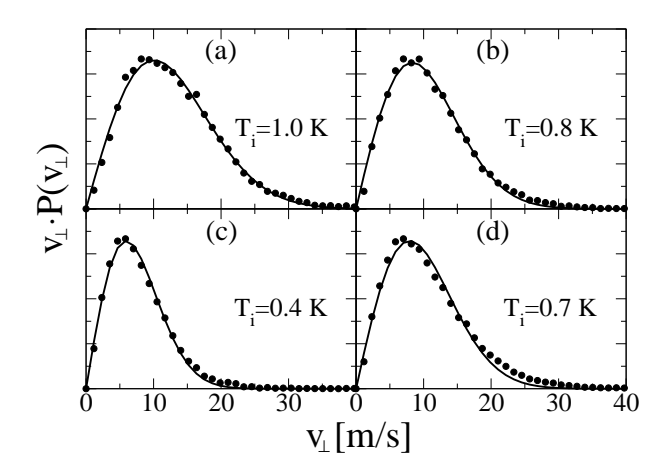


FIG. 7: Same as Fig. 6, but for  $t = 1.5 \,\mu\text{s}$ .

dynamics of the plasma. For comparing the kinetic model with the H-MD calculations, the very definition of  $T_i$  for the MD simulation requires some discussion. As discussed in section II, we assume a Gaussian velocity distribution, i.e. a well-defined temperature  $T_i$ , for the plasma ions in our kinetic model. This, of course, is an approximation since the plasma is not created in an equilibrium state. The total kinetic energy of the ions is a sum of the hydrodynamical expansion energy and a contribution due to the thermal motion of the ions. Since the hydrodynamical velocity is directed radially (Eq. (14)), we determine the thermal energy of the ions from the average of the velocity component perpendicular to the radial direction

$$k_{\rm B}T_{\rm i} = \frac{m_{\rm i}}{2} \left\langle \left(\frac{\mathbf{v} \times \mathbf{r}}{r}\right)^2 \right\rangle = \frac{m_{\rm i}}{2} \left\langle v_{\perp}^2 \right\rangle .$$
 (25)

Clearly, such an assignment of a temperature to the average velocity is only well defined if the ion velocities  $v_{\perp}$  are distributed according to a Maxwell distribution. In order to check the validity of this requirement, we have sampled the ion velocity distribution  $v_{\perp}$  from three different regions in the plasma:  $r \leq 1.3\sigma$ ,  $1.3\sigma < r \leq 2\sigma$ , and  $r > 2\sigma$ , which have been chosen so that each region is occupied by approximately the same number of ions. The resulting distributions are plotted at two different times  $t = 0.3 \,\mu\text{s} = 1.3\omega_{\text{p,i}}^{-1}$  and  $t = 1.5 \,\mu\text{s} = 7\omega_{\text{p,i}}^{-1}$  in Figs. 6 and 7, respectively. Additionally, we have fitted a Maxwell-Boltzmann distribution to the numerical results, formally defining a temperature in the corresponding plasma region. As can be seen in Fig. 6, even at the very early stage of the plasma evolution the numerical data is well fitted by an equilibrium distribution in the inner plasma region, while there are deviations in the outer region of the plasma since the relaxation time is longer

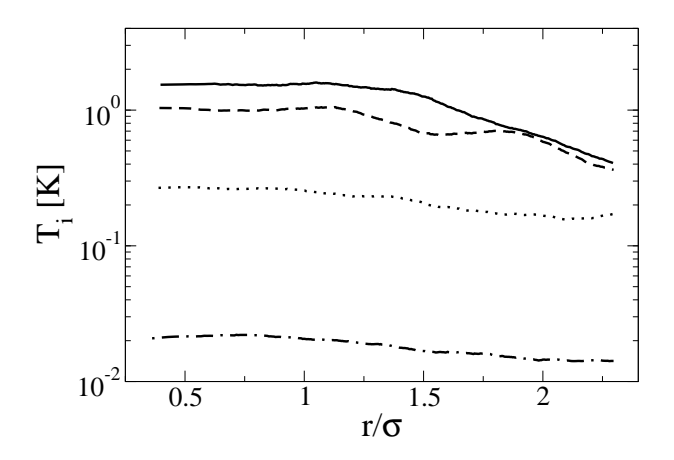


FIG. 8: Average thermal ionic energy as a function of the distance from the plasma center at four different times:  $t = 0.3 \,\mu\text{s}$  (solid),  $t = 1.5 \,\mu\text{s}$  (dashed),  $t = 6.0 \,\mu\text{s}$  (dotted) and  $t = 25.3 \,\mu\text{s}$  (dot-dashed). Initial-state parameters are the same as in Fig. 1.

due to the lower density far away from the plasma center. However, already after a relatively short time of  $t = 1.5 \,\mu$ s the velocity distributions are well fitted by a Maxwell-Boltzmann distribution in all three plasma regions (Fig. 7). Hence, the ion thermal energy can be represented by a local temperature  $T_i(r)$ , decreasing with growing distance from the plasma center as can be seen from Figs. 6 and 7. This is due to the fact that the initial heating arises from a compensation of the negative correlation energy, which is larger in the central plasma region where the density is higher. However, as becomes apparent by comparing Figs. 6 and 7, the thermal energy equilibrates over the whole plasma volume rather quickly as the system evolves. While the temperatures defined in the inner and outermost region deviate by a factor of eight at  $t = 0.3 \,\mu$ s, they differ by a factor of two only 1.2  $\mu$ s later.

Figure 8 gives a more detailed account of this equilibration process. Here, the local ionic temperature is plotted as a function of the radial distance from the plasma center at four different times, where  $T_i(r)$  has been defined from the velocity average of a shell of 2000 ions with a central shell radius r. The temperature decrease with increasing distance from the center as discussed above is clearly visible. Nevertheless, the ion temperature is seen to equilibrate rather quickly, so that the approximation of a homogeneous ion temperature, used in the derivation of the kinetic model in section II A, becomes better and better at later times. Moreover, the numerically calculated distribution of thermal velocities sampled over the whole plasma volume is well represented by a Maxwell-Boltzmann distribution with some average temperature intermediate between the temperatures of the inner and outer region,

respectively (Fig. 7d). This shows that the Gaussian phase-space distribution assumed for the ions in section II A agrees very well with the results of the MD simulation averaged over the spatial coordinates, even if the temperature still shows substantial inhomogeneities.

### C. Spatially averaged ionic observables

As we have demonstrated in section III A the kinetic model describes the global temporal evolution of the plasma including recombination quite accurately. From the detailed analysis of the spatially resolved plasma dynamics in the previous subsection we may expect that the kinetic model describes spatially averaged observables, such as the kinetic energy of the expansion, the thermal energy, and the correlation energy of the plasma quite well. This is indeed the case over almost the entire evolution time as Fig. 9 demonstrates for the correlation energy and the thermal ion energy. Only at an early stage of the plasma evolution, differences between MD simulation and kinetic model are visible, showing that the correlation-time approximation Eq. (17) does not accurately describe this early phase of equilibration starting from a completely uncorrelated state in all details. Since the initial state is very far from equilibrium, the initial relaxation process is not exponential, as assumed in the correlation-time approximation Eq. (17). Rather, it is connected with transient oscillations of the temperature (inset of Fig. 9) which have been found both theoretically [18, 33, 34] and experimentally [35]. However, the timescale of the initial ion heating as well as the maximum temperature are well reproduced by the simple model. After the system has come sufficiently close to local equilibrium, the quality of the correlation-time approximation becomes better and, once again, close agreement between the two approaches is found, supporting our argument put forward in the derivation of the kinetic approach in section II. At later times differences become apparent, which may be attributed to the fact that the ion relaxation is considerably disturbed by recombination and ionization events leading to sudden local changes of the charge density, which is not taken into account by the kinetic model.

Furthermore, according to both approaches, the correlation energy and the thermal kinetic energy of the ions are almost identical roughly to the time where both curves reach their maximum values, showing that the total correlation energy is completely converted into thermal kinetic energy of the ions, as expressed by Eq. (15c). At later times, this addi-

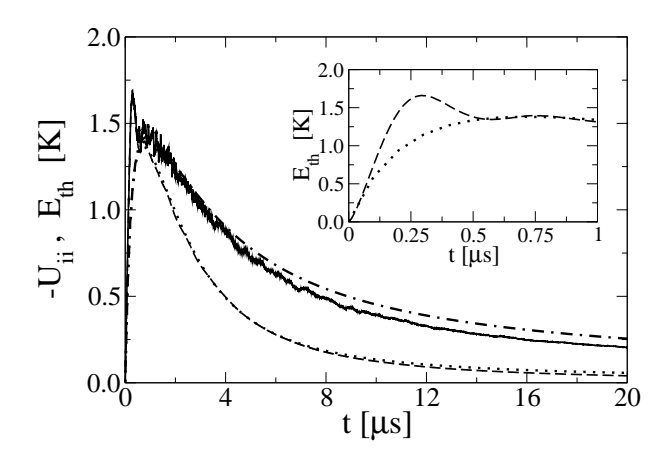


FIG. 9: Correlation energy (solid line: H-MD simulation, dot-dashed: kinetic result) and thermal ion kinetic energy (dashed: H-MD, dotted: kinetic). Initial-state parameters are the same as in Fig. 1. The inset shows the ion thermal energy in the early stage of the relaxation process with its characteristic transiently oscillatory behavior.

tional kinetic energy is transferred to the outward directed motion of the ions, leading to an indirect enhancement of the plasma expansion by the development of IC and to adiabatic cooling of the ions. Therefore, the thermal ion kinetic energy starts to deviate from the correlation energy as the plasma expansion sets in.

### IV. CONCLUSIONS

In summary, we have presented two different theoretical approaches for the simulation of ultracold neutral plasmas. First, we have introduced a simple kinetic model along the lines of [10], and we have shown how to include a description of IC into the model in an approximate way. Moreover, we have developed a hybrid molecular dynamics approach which allows for an accurate description of the strongly coupled ion motion on microsecond timescales, by treating the electronic component as a fluid using an adiabatic approximation while the ions are fully accounted for on an MD level.

Supporting our results from [13], both methods show that the inclusion of IC enhances the number of recombined Rydberg atoms by a few percent, but only slightly affects the macroscopic expansion dynamics of the plasma itself. As we have shown, this is due to the fact that mainly the population of very highly excited states is increased if IC are taken into account, which have a small binding energy and therefore hardly influence the electron

temperature.

By comparison of the two methods, we could show that the simple kinetic description adequately describes the evolution of global, i.e. spatially averaged, plasma observables. Thus, the kinetic model, which allows for a much faster computation, may be used to quickly and efficiently scan the vast space of initial-state parameters, e.g. in order to obtain a "phase diagram" for Rydberg gas / plasma systems [36]. Moreover, it permits extending the description of ultracold plasmas to a parameter range where the plasma is so large that the number of particles  $(N_i \gtrsim 10^6)$  prohibits an MD simulation. Maybe even more importantly, the simple kinetic equations give additional insight into the dynamics beyond that possible on the basis of MD simulations by providing simple evolution equations for the macroscopic parameters describing the plasma state.

On the other hand, spatially resolved quantities such as ionic density, ion velocities or local temperature show deviations from the behavior predicted by the simple kinetic model. However, the developed H-MD approach provides a powerful method for the study of these quantities, and for the detailed description of the relaxation dynamics of the strongly coupled ions on a microsecond timescale. Moreover, it permits the study of scenarios where the ions are so strongly coupled that Coulomb crystallization occurs [16], which cannot be described by the kinetic model.

# Acknowledgments

We gratefully acknowledge helpful discussions with T.C. Killian and F. Robicheaux. This work was supported by the DFG within the Priority Programme SPP1116 (Grant-No. RO1157/4).

### APPENDIX A: DERIVATION OF THE CORRELATION FORCE

In this section, the approximation Eq. (12) for  $\mathbf{F}_{ii}$  is derived. We start from Eq. (7)

$$\mathbf{F}_{ii} = e^2 \int \rho_i(\mathbf{r}') g_{ii}(\mathbf{r}, \mathbf{r}') \frac{\mathbf{r} - \mathbf{r}'}{|\mathbf{r} - \mathbf{r}'|^3} d\mathbf{r}' , \qquad (A1)$$

where the explicit expression  $\varphi_{ii} = e^2/|\mathbf{r} - \mathbf{r}'|$  for the inter-ionic Coulomb potential has been inserted. In general, the correlation function  $g_{ii}$  is a function of both coordinates  $\mathbf{r}$  and  $\mathbf{r}'$ .

However, in the case of a homogeneous density,  $g_{ii}$  depends only on the interparticle distance  $x = |\mathbf{r} - \mathbf{r}'|$ . Since the relevant property which distinguishes the two points  $\mathbf{r}$  and  $\mathbf{r}'$  is the corresponding density (from the way the plasma is created, no other differences, e.g. that part of the plasma would be in a state with equilibrium correlations while a different part would be totally uncorrelated, are apparent), it seems a reasonable approximation to assume that the space dependence of the correlation function enters only via the densities at the respective coordinates [37]. Hence, we write the correlation function as

$$g_{ii}(\mathbf{r}, \mathbf{r}') \approx g_{ii} \left[ \rho_i(\mathbf{r}), \rho_i(\mathbf{r}'), |\mathbf{r} - \mathbf{r}'| \right]$$
 (A2)

With the substitution  $\mathbf{r}' = \mathbf{r} + \mathbf{x}$ , Eq. (A1) becomes

$$\mathbf{F}_{ii} = -e^2 \int \rho_i(\mathbf{r} + \mathbf{x}) g_{ii} \left[ \rho_i(\mathbf{r}), \rho_i(\mathbf{r} + \mathbf{x}), x \right] \frac{\mathbf{x}}{x^3} d\mathbf{x} . \tag{A3}$$

Since the correlation function rapidly decreases for distances x larger than the correlation length  $\lambda_c$ , we may restrict the integration in Eq. (A3) to a sphere with a radius of approximately  $\lambda_c$ . If the plasma density does not vary strongly on the scale of the correlation length, we may use a linear Taylor expansion of the density

$$\rho_{\rm i}\left(\mathbf{r} + \mathbf{x}\right) \approx \rho_{\rm i}\left(\mathbf{r}\right) + \mathbf{x} \cdot \nabla \rho_{\rm i}\left(\mathbf{r}\right)$$
(A4)

and the correlation function

$$g_{ii}(\rho_{i}, \rho'_{i}, x) = g_{ii}(\rho_{i}, \rho_{i}, x) + \frac{\partial g_{ii}(\rho_{i}, \rho'_{i}, x)}{\partial \rho'_{i}} \bigg|_{\rho'_{i} = \rho} (\mathbf{x} \cdot \nabla \rho_{i}) , \qquad (A5)$$

where  $\rho_i = \rho_i(\mathbf{r})$  and  $\rho_i' = \rho_i(\mathbf{r} + \mathbf{x})$ .

Substitution of Eq. (A4) and Eq. (A5) into Eq. (A3) and keeping only terms up to linear order in  $\mathbf{x} \cdot \nabla \rho_i$  yields

$$\mathbf{F}_{ii} = -e^2 \left( \int \frac{\mathbf{x}}{x^3} \, \rho_i \, g_{ii}(\rho_i, x) \, d\mathbf{x} + \int \frac{\mathbf{x}}{x^3} \, g_{ii}(\rho_i, x) \, \left( \mathbf{x} \cdot \nabla \rho_i \right) \, d\mathbf{x} + \frac{1}{2} \int \frac{\mathbf{x}}{x^3} \, \rho_i \, \frac{\partial g_{ii}(\rho_i, x)}{\partial \rho_i} \, \left( \mathbf{x} \cdot \nabla \rho_i \right) \, d\mathbf{x} \right) \,, \tag{A6}$$

where  $g_{ii}(\rho_i, x) \equiv g(\rho_i, \rho'_i, x)|_{\rho'_i = \rho_i}$  and we have used the relation

$$\frac{\partial}{\partial \rho_{i}} \left( g_{ii}(\rho_{i}, \rho'_{i}, x) |_{\rho'_{i} = \rho_{i}} \right) = \left. \frac{\partial g(\rho_{i}, \rho'_{i}, x)}{\partial \rho_{i}} \right|_{\rho'_{i} = \rho_{i}} + \left. \frac{\partial g_{ii}(\rho_{i}, \rho'_{i}, x)}{\partial \rho'_{i}} \right|_{\rho'_{i} = \rho_{i}} = 2 \left. \frac{\partial g(\rho_{i}, \rho'_{i}, x)}{\partial \rho'_{i}} \right|_{\rho'_{i} = \rho_{i}}, \tag{A7}$$

which follows from the symmetry of  $g_{ii}$  under particle exchange, i.e., under exchange of  $\rho_i$  and  $\rho'_i$ . Since the integrand of the first integral in Eq. (A6) is an odd function in  $\mathbf{x}$  the first term vanishes. The second term yields after some manipulations

$$e^{2} \int \frac{\mathbf{x}}{x^{3}} g_{ii}(\rho_{i}, x) \left(\mathbf{x} \cdot \nabla \rho_{i}\right) d\mathbf{x} = \frac{e^{2}}{3} \nabla \rho_{i} \int \frac{g_{ii}(\rho_{i}, x)}{x} d\mathbf{x}.$$
 (A8)

Analogously, the third term can be written as

$$\frac{e^2}{2} \int \frac{\mathbf{x}}{x^3} \rho_i \frac{\partial g_{ii}(\rho_i, x)}{\partial \rho_i} (\mathbf{x} \cdot \nabla \rho_i) d\mathbf{x} = \frac{e^2}{6} \rho_i \nabla \rho_i \frac{\partial}{\partial \rho_i} \int \frac{g_{ii}(\rho_i, x)}{x} d\mathbf{x},$$
 (A9)

which together leads to

$$\mathbf{F}_{ii} = -\frac{e^2}{6} \, \nabla \rho_i \, \left[ \int \frac{g_{ii}(\rho_i, x)}{x} \, d\mathbf{x} + \, \frac{\partial}{\partial \rho_i} \left( \rho_i \int \frac{g_{ii}(\rho_i, x)}{x} \, d\mathbf{x} \right) \right]. \tag{A10}$$

Finally, substitution of the definition of the correlation energy u as given by Eq. (13) yields the result Eq. (12). An analogous calculation for the expression of the correlation energy Eq. (9) leads to the familiar LDA result [37]

$$U_{ii} = \frac{e^2}{2N_i} \int \rho_i(\mathbf{r}) \rho_i(\mathbf{r}') g_{ii}(\mathbf{r}, \mathbf{r}') \frac{1}{|\mathbf{r} - \mathbf{r}'|} d\mathbf{r}' d\mathbf{r}$$
$$= N_i^{-1} \int \rho_i u_{ii} d\mathbf{r} . \tag{A11}$$

 T.C. Killian, S. Kulin, S.D. Bergeson, L.A. Orozco, C. Orzel and S.L. Rolston, Phys. Rev. Lett. 83, 4776 (1999).

- [4] M.P. Robinson, B.L. Tolra, M.W. Noel, T.F. Gallagher and P. Pillet, Phys. Rev. Lett. 85, 4466 (2000).
- [5] E. Eyler, A. Estrin, J.R. Ensher, C.H. Cheng, C. Sanborn P.L. Gould, Bull. Am. Phys. Soc. 45, 56 (2000).
- [6] P.L. Gould, S.M. Farooqi, S. Krishnan, J. Stanojevic, D. Tong, Y.P. Zhang, J.R. Ensher, A. Estrin, C.-H. Cheng and E.E. Eyler, in *Interactions in Ultracold Gases: From Atoms to Molecules*, eds. M. Weidemüller and C. Zimmermann (Wiley-VCH, 2003), p. 270.

<sup>[2]</sup> S. Kulin, T.C. Killian, S.D. Bergeson and S.L. Rolston, Phys. Rev. Lett. 85, 318 (2000).

<sup>[3]</sup> T.C. Killian, M.J. Lim, S. Kulin, R. Dumke, S.D. Bergeson and S.L. Rolston, Phys. Rev. Lett. 86, 3759 (2001).

- [7] S.G. Kuzmin and T.M. O'Neil, Phys. Rev. Lett. 88, 065003 (2002).
- [8] S.G. Kuzmin and T.M. O'Neil, Phys. Plasmas 9, 3743 (2002).
- [9] S. Mazevet, L.A. Collins and J.D. Kress, Phys. Rev. Lett. 88, 055001 (2002).
- [10] F. Robicheaux and J.D. Hanson, Phys. Rev. Lett. 88, 055002 (2002).
- [11] F. Robicheaux and J.D. Hanson, Phys. Plasmas 10, 2217 (2003).
- [12] A.N. Tkachev and S.I. Yakovlenko, Quantum Electronics 31, 1084 (2001).
- [13] T. Pohl, T. Pattard and J.M. Rost, Phys. Rev. A 68, 010703(R) (2003).
- [14] D.H.E. Dubin and T.M. O'Neil, Rev. Mod. Phys. **71**, 87 (1999).
- [15] S. Ichimaru, Rev. Mod. Phys. **54**, 1017 (1982).
- [16] T. Pohl, T. Pattard and J.M. Rost, Phys. Rev. Lett. 92, 155003 (2004).
- [17] M.S. Murillo, Phys. Rev. Lett. 87, 115003 (2001).
- [18] T. Pohl, T. Pattard and J.M. Rost, J. Phys. B 37, L183 (2004).
- [19] D.S. Dorozhkina and V.E. Semenov, Phys. Rev. Lett. 81, 2691 (1998).
- [20] D. Semkat, D. Kremp and M. Bonitz, Phys. Rev. E **59**, 1557 (1999).
- [21] M. Bonitz, Phys. Lett. A **221**, 85 (1996).
- [22] M. Bonitz and D. Kremp, Phys. Lett. A **212**, 83 (1996).
- [23] K. Morawetz, V. Spicka, P. Lipavský, Phys. Lett. A 246, 311 (1998).
- [24] G. Chabrier and A.Y. Potekhin, Phys. Rev. E 58, 4941 (1998).
- [25] P. Mansbach and J. Keck, Phys. Rev. **181**, 275 (1969).
- [26] S. Chandrasekhar, Astrophys. J. 98, 54 (1943).
- [27] I.R. King, Astron. J. **71**, 64 (1966).
- [28] J.E. Barnes and P. Hut, Nature **324**, 446 (1986).
- [29] J.E. Barnes, J. Comp. Phys. 87, 161 (1990).
- [30] C.K. Birdsall and A.B. Langdon, *Plasma physics via computer simulation* (Bristol: Inst. of Physics Publ., 1995).
- [31] A.V. Gurevich, L.V. Pariiskaya and L.P. Pitaevskii, Soviet Phys. JETP 22, 449 (1966)
- [32] C. Sack and H. Schamel, Plasma. Phys. Contr. F. 27, 717 (1985).
- [33] G. Zwicknagel, Contrib. Plasma Phys. **39**, 155 (1999).
- [34] I.V. Morozov, G.E. Norman, J. Phys. A 36, 6005 (2003).
- [35] T.C. Killian, private communication (2004).
- [36] T. Pattard, T. Pohl and J.M. Rost, Few-Body Systems, in press (2004).

[37] R. Evans, Adv. Phys. 28, 143 (1979).